

Theory of internal conversion of the ^{229}Th nuclear isomer in solid-state hosts

H. W. T. Morgan,^{1,2} H. B. Tran Tan,^{3,4} R. Elwell,⁵ A. N. Alexandrova,¹ Eric R. Hudson,^{5,6,7} and Andrei Derevianko^{3,*}

¹Department of Chemistry and Biochemistry, University of California, Los Angeles, Los Angeles, CA 90095, USA

²Department of Chemistry, University of Manchester, Oxford Road, Manchester M13 9PL, UK

³Department of Physics, University of Nevada, Reno, Nevada 89557, USA

⁴Los Alamos National Laboratory, P.O. Box 1663, Los Alamos, New Mexico 87545, USA

⁵Department of Physics and Astronomy, University of California, Los Angeles, CA 90095, USA

⁶Challenge Institute for Quantum Computation, University of California Los Angeles, Los Angeles, CA, USA

⁷Center for Quantum Science and Engineering, University of California Los Angeles, Los Angeles, CA, USA

(Dated: November 26, 2024)

Laser excitation of ^{229}Th nuclei in doped wide bandgap crystals has been demonstrated recently, opening the possibility of developing ultrastable solid-state clocks and sensitive searches for new physics. We develop a quantitative theory of the internal conversion of isomeric ^{229}Th in solid-state hosts. The internal conversion of the isomer proceeds by resonantly exciting a valence band electron to a defect state, accompanied by multi-phonon emission. We demonstrate that, if the process is energetically allowed, it generally quenches the isomer on timescales much faster than the isomer's radiative lifetime, despite thorium being in the +4 charge state in the valence band.

The laser-accessible 8.4 eV isomeric transition in ^{229}Th nucleus holds an intriguing promise for developing quantum technologies and fundamental physics searches based on coherent manipulation of *nuclear* degrees of freedom. In particular, a crystal doped with a macroscopic number of ^{229}Th nuclei enables realizing a portable frequency standard with an unprecedented degree of stability - a solid-state nuclear clock [1]. Observations of direct laser excitation of ^{229}Th in three distinct solid-state hosts have been reported recently [2–5].

There is presently great need for a quantitative theoretical understanding of processes in these novel systems so that they may be optimized. The challenge lies in bridging concepts and techniques from distinct sub-fields: materials science, quantum chemistry, condensed matter physics, nuclear physics, and atomic and optical physics. In particular, one of the critically important decay channels in nuclei in a chemical environment is the internal conversion (IC) channel, see Fig. 1. During IC, the nucleus relaxes non-radiatively by transferring its energy to the environment. As such, IC is practically important, as it competes with the radiative nuclear decay channel and can greatly affect clock performance. While IC in a free ^{229}Th atom and its ions has been understood quantitatively [6–9], the IC theory of ^{229}Th ions in a crystal environment has been lacking [10]. This work aims to fill this gap.

There are contradicting qualitative arguments in the literature regarding the relative importance of the IC process in solid-state hosts. For example, Ref. [2] states “since the nuclei are present in the Th^{4+} charge state, we do not expect a significant contribution of bound internal conversion to the decay rate.” Meanwhile, Ref. [3] postulates a quenching mechanism due to electronic defect states introduced into the crystal in the thorium doping process and presents preliminary experimental evidence

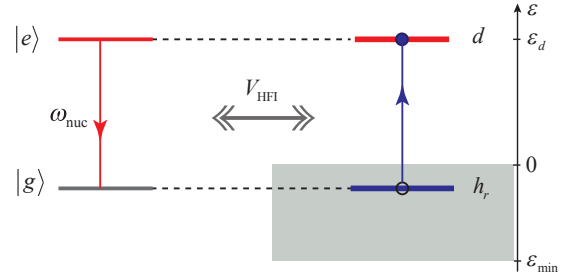


FIG. 1. During the internal conversion in a crystal, a ^{229}Th nucleus relaxes non-radiatively by resonantly transferring its $\omega_{\text{nuc}} \approx 8.4\text{ eV}$ energy to a particle-hole ($d - h_r$) electronic excitation. The hole state h_r lies in the valence band, while the defect state d lies inside the bandgap. The excitation transfer is mediated by V_{HFI} , the hyperfine coupling between the nuclear and electronic degrees of freedom. The valence band is shown as a gray box, with the valence band maximum at $\varepsilon = 0$ and the minimum at ε_{min} .

in support of significant quenching; likewise the results of Ref. [11] may be interpreted to support the presence of non-radiative decay. Here, we analyze the situation theoretically and show that, if energetically allowed, the IC process is possible and can in fact be the dominant decay channel in ^{229}Th -doped crystals. We develop a general framework by combining the widely used density functional theory (DFT) with the *ab initio* relativistic treatment of electron interactions with the ^{229}Th nucleus, capturing the important ingredients of IC in ^{229}Th -doped solid-state hosts.

In solid-state ^{229}Th experiments, suitable host crystals are insulators, with band-gaps larger than the nuclear transition frequency $\omega_{\text{nuc}} \approx 8.4\text{ eV}$ so that the crystals are transparent to VUV radiation [1] – ThF_4 in Ref. [4], LiSrAlF_6 in Ref. [3], and CaF_2 in [2, 5]. Doping ^{229}Th into LiSrAlF_6 and CaF_2 generically creates spatially-

localized electronic defect states with typical energies inside the insulator gap, as shown in Fig. 1.

The electronic energies and wavefunctions (including those of defect states) in solid state materials may be obtained by solving the eigenvalue equation

$$h_{\text{el}}(\mathbf{r})\phi_i(\mathbf{r}) = \varepsilon_i\phi_i(\mathbf{r}), \quad (1)$$

where $h_{\text{el}}(\mathbf{r})$ is a suitably chosen self-consistent field electronic Hamiltonian and ϕ_i are single-electron orbitals. In materials science, density functional theory (DFT) is widely used to handle Eq. (1). Kohn-Sham DFT gives orbitals ϕ_i for the valence band and the defect at a fixed lattice and doping geometry, and all orbitals are orthogonalized during the calculation. For more details on our use of DFT in $^{229}\text{Th}:\text{LiSrAlF}_6$ see the supplementary information.

The valence band is fully occupied and in the second quantization it can be represented by the quasi-vacuum state $|\Omega\rangle = \left(\prod_{\varepsilon_i < 0} a_i^\dagger\right)|0\rangle$, where we placed the zero of energies ε_i at the valence band maximum. The electronic Hamiltonian may be written as $H_{\text{el}} = \sum_k h_{\text{el}}(\mathbf{r}_k) = \sum_i \varepsilon_i : a_i^\dagger a_i :$. Here a^\dagger and a are the fermionic creation and annihilation operators and $:\dots:$ stands for the conventional normal ordering of operator products [12] with respect to the quasi-vacuum state $|\Omega\rangle$. The summation with i extends over the entire single-electron spectrum $\{\varepsilon_i\}$. Of particular interest for this work are states where a valence electron is excited into a defect state above the Fermi level, leaving behind a ‘‘hole’’. A particle-hole excitation from the valence band to the defect state d reads $a_d^\dagger a_h |\Omega\rangle$. The energy of this particle-hole excitation is $\varepsilon_d - \varepsilon_h$.

Here, the nuclear subsystem is modeled as two distinct energy levels: the ground state $|g\rangle$ with nuclear spin $I_g = 5/2$ and the excited (isomeric) state $|e\rangle$ with $I = 3/2$, separated by the energy gap ω_{nuc} . Fixing the energy of the nuclear ground state at zero, the unperturbed nuclear Hamiltonian reduces to $H_{\text{nuc}} = \omega_{\text{nuc}}|e\rangle\langle e|$, with an implicit summation over nuclear magnetic sublevels, m_I . Unless specified otherwise, atomic units, $|e| = \hbar = m_e \equiv 1$, are used throughout.

The Hilbert space of the compound electron-nuclear system is spanned by the tensor product of the nuclear and electronic states with the absolute ground state of the compound system, $H_0 = H_{\text{el}} + H_{\text{nuc}}$, written as $|\Psi_0^g\rangle = |\Omega\rangle|g\rangle$. The nuclear and electronic degrees of freedom are coupled via the hyperfine interaction (HFI) V_{HFI} and the total Hamiltonian of the compound system reads $H = H_{\text{el}} + H_{\text{nuc}} + V_{\text{HFI}}$, with

$$V_{\text{HFI}} = \sum_{ij} \sum_{n'n} V_{ij}^{n'n} : a_i^\dagger a_j : |n'\rangle\langle n|, \quad (2)$$

where indices i and j range over the single-electron spectrum (1) and n and n' run over the nuclear states $|e\rangle$ and

$|g\rangle$. Phononic degrees of freedom are suppressed in this expression, but included in the calculations that follow.

The main task for analyzing the impact of IC decay is to understand the lifetime of the nuclear state in a crystalline environment. Thus, our aim is to calculate the lifetime of the state, $|\Psi_0^e\rangle = |\Omega\rangle|e\rangle$, with the nucleus in the isomeric state $|e\rangle$ and all the electrons occupying the valence band, which has energy $E_0^e = \omega_{\text{nuc}}$. Such a state is embedded into the continuum of particle-hole states

$$|\Psi_{dh}^g\rangle = a_d^\dagger a_h |\Omega\rangle|g\rangle, \quad E_{dh}^g = \varepsilon_d - \varepsilon_h \quad (3)$$

with the nucleus in its ground state, an electron in the defect state, and a hole in the valence band. Given the valence band is a continuum, typically one of these states, denoted as $|\Psi_{dh_r}^g\rangle$ where h_r is the resonant hole (see Fig. 1) has an energy of

$$E_{dh_r}^g = \varepsilon_d - \varepsilon_{h_r} = \omega_{\text{nuc}}, \quad (4)$$

and is therefore degenerate with $|\Psi_0^e\rangle$.

In the illustrative model of Fig. 1, the discrete spectrum contains a single defect state. Since the zero of electronic energy is defined at the valence band maximum (i.e., the Fermi level), the energy of the hole must satisfy $\varepsilon_{h_r} \leq 0$. As a result, the resonance condition (4) is only met if the defect lies at or below the nuclear excitation on the energy diagram, leading to the requirement:

$$\varepsilon_d \leq \omega_{\text{nuc}}. \quad (5)$$

In addition, the energy of the resonant hole must lie within the valence band, implying

$$\varepsilon_d - \varepsilon_{\text{min}} \geq \omega_{\text{nuc}}, \quad (6)$$

where ε_{min} is the valence band minimum, see Fig. 1.

This model maps onto a textbook problem [13], where a discrete state $|\Psi_0^e\rangle$ is embedded into the $|\Psi_{dh}^g\rangle$ continuum. These are coupled by a time-independent perturbation V_{HFI} . As a result, the $|\Psi_0^e\rangle$ state decays into the continuum, relaxing the nucleus, and generating a particle-hole pair. This is an internal conversion (IC) mechanism in the solid-state hosts. The rate of this decay is given by Fermi’s golden rule [14]

$$\begin{aligned} \Gamma_{\text{IC}} &= \frac{2\pi}{\hbar} \rho(\varepsilon_{h_r}) |\langle \Psi_{dh_r}^g | V_{\text{HFI}} | \Psi_0^e \rangle|^2 \\ &= \frac{2\pi}{\hbar} \rho(\varepsilon_{h_r} = \varepsilon_d - \omega_{\text{nuc}}) |V_{dh_r}^{ge}|^2, \end{aligned} \quad (7)$$

with $\rho(\varepsilon_{h_r})$ being the electronic density of states (DOS) at the resonant hole energy.

The decay rate (7) assumes a single defect state. For a manifold $\{d_i\}$ of defect states, the rate is summed over all available decay channels. Summing over the nuclear

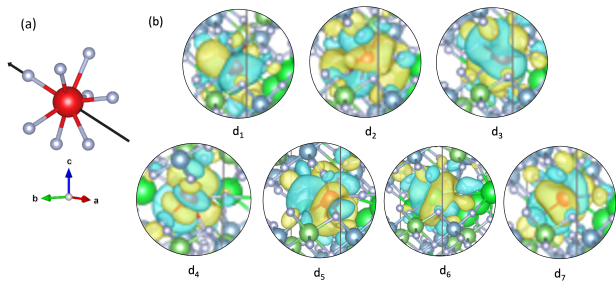


FIG. 2. (a) ThF₈ cluster from the optimized structure of Th:LiSrAlF₆ annotated with the vector (0.01, 0.135, 0.065) in black in fractional coordinates, which is a vector from the Th atom to one of the nearest-neighbor F atoms. (b) Real-space wavefunctions of the Th defect states evaluated at the Γ point. These closely resemble 5*f* electronic orbitals. Th atoms are shown in red, Li in dark green, Sr in bright green, Al in blue, and F in grey. Blue and yellow isosurfaces represent the real part of the wavefunction - in all cases the imaginary part appears identical.

magnetic quantum numbers m_g of the final state and averaging over magnetic quantum numbers m_e of the initial nuclear state, the rate becomes:

$$\Gamma_{\text{IC}} = \frac{2\pi}{2I_e + 1} \sum_{d_i} \sum_{h_r} \rho(\varepsilon_{h_r} = \varepsilon_{d_i} - \omega_{\text{nuc}}) \times \sum_{m_e m_g} |V_{d_i h_r}^{g m_g e m_e}|^2. \quad (8)$$

Here, the energy selection rules (5,6) are included implicitly, as the DOS vanishes if these conditions are violated.

For concreteness, we evaluate the IC rates for Th-doped LiSrAlF₆ and CaF₂. The technique we develop below applies to a broad class of Th-doped VUV transparent solid-state hosts. The electronic structure of Th-doped LiSrAlF₆ is computed within DFT using the Vienna Ab initio Simulation Package (VASP) [15]. Details are provided in Ref. [3] and the supplementary information. We consider a doping geometry with one Th atom substituted into a Sr site and two additional interstitial F atoms (for charge compensation). Such a doping geometry yields the lowest energy among various possible site substitutions. These calculations find that the lowest-energy unoccupied orbitals are a closely-spaced manifold of seven states $\{d_i\}$ resembling the 5*f* orbitals $\psi_{5f_m}(\mathbf{r})$ of thorium (here m denotes the magnetic quantum number). Fig. 2 shows real-space representations of these orbitals. The Th 6*d* orbitals appear above the 5*f* orbitals. In the ground electronic state these orbitals are empty, so Th is in the +4 oxidation state. In the excited electronic state $|\Psi_{dh}\rangle$ an electron is transferred from F into the Th 5*f* manifold, putting Th into the +3 oxidation state. This is evidenced by the 5*f*-like unoccupied states in shown in Fig. 2 and the predominant F 2*p* character of the valence band shown in the PDOS in Fig. S1.

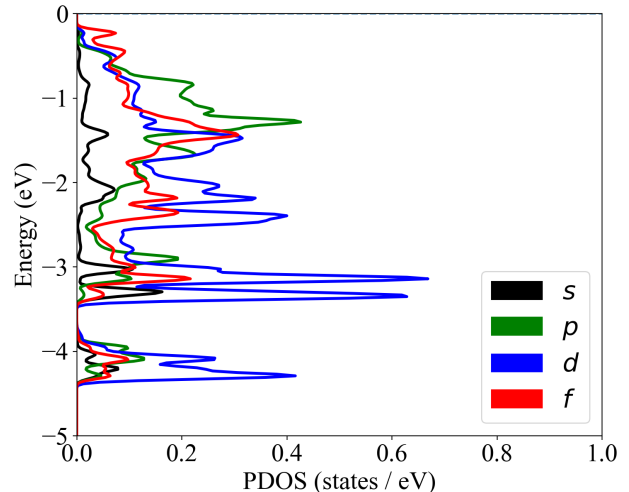


FIG. 3. Thorium projected density of states in the valence band for Th:LiSrAlF₆.

An IC-induced excitation of the valence band electron to the defect state is accompanied by a charge transfer from F to the Th ion. This leads to electrostatic distortion of the lattice, see supplementary information. In a molecular picture of the defect, the vibrational state of the ThF_n “cluster” is significantly excited after nuclear relaxation, leading to multi-phonon relaxation. The evaluation of $V_{dh_r}^{ge}$ must therefore include the phononic degree of freedom. We analyze the phononic part of the matrix element within the Huang-Rhys approximation [16]. Based on the computed relaxation energy in ²²⁹Th:LiSrAlF₆ of $E_R \approx 0.5$ eV and phonon frequencies, we find the $V_{dh_r}^{ge}$ is modified by a factor of order unity. Therefore, the IC rate expression (8) at low temperatures is valid without including phononic effects, but with the defect energies shifted by the relaxation energy $\varepsilon_{d_i} \rightarrow \varepsilon_{d_i} - E_R$. In the following, this shift is suppressed for brevity.

We repeated the DFT calculations for Th:CaF₂, using the geometry with two interstitial fluorides at 90° that was previously shown to be the lowest energy thorium defect [17]. PDOS plots for Th and F in Figs. S2-4 show that the electronic structure of thorium is qualitatively similar in Th:CaF₂ and Th:LiSrAlF₆ and that both will undergo F-Th electron transfer excitations. In Th:CaF₂ we also find the Th 5*f*-like orbitals to be the lowest unoccupied orbitals, with Th in the +4 oxidation state. This motivates our treatment of the electronic defect states as resembling the Th³⁺ 5*f* orbitals $\psi_{5f_m}(\mathbf{r})$. Indeed, the 4*f* orbitals are included in the frozen core of thorium, while the energies of the 6*f*, 7*f*, ... orbits are too high to contribute significantly to the valence band.

The HFI matrix element in Eq. (8) may be decomposed into a scalar product of the electronic and nuclear tensors

of various ranks [18].

$$V_{dh_r}^{ge} = \langle g|\boldsymbol{\mu}|e\rangle \cdot \langle d|\mathbf{T}|h_r\rangle, \quad (9)$$

where $\boldsymbol{\mu}$ is the nuclear M1 operator and \mathbf{T} is an electronic operator. Inclusion of the higher-rank electric-quadrupole HFI would only increase the IC rate, strengthening the conclusions of our work.

Since the HFI matrix element is accumulated near the nucleus, we are interested in components of the valence band hole state centered on the thorium impurity. As the defect state is predominantly of the $5f$ character, we are interested in the f content of the hole state due to the HFI selection rules (\mathbf{T} is a rank 1 parity-even tensor). To this end, one may carry out a partial wave expansion,

$$\phi_h(\mathbf{r}) = \sum_{m_h} c_{5f m_h}^h \psi_{5f m_h}(\mathbf{r}) + \dots, \quad (10)$$

where ellipses denote remaining contributions to the valence orbital ϕ_h . In general, the p admixtures in (10) can also contribute to the IC rate, but the HFI matrix elements between the p and f orbitals vanish non-relativistically and thereby contribute at a smaller level.

In principle, the expansion coefficients may be found using $c_{5f m}^h = \int d^3r \psi_{5f m}^*(\mathbf{r}) \phi_h(\mathbf{r})$. This, however, requires detailed knowledge of the valence band wavefunctions at distances comparable to the atomic size. At these sub-Bohr-radius scales, VASP utilizes pseudo-potentials that do not capture the correct behavior of atomic orbitals. Instead, we notice that the projected density of states (PDOS) in the valence band for the f -orbital character reads

$$\rho_f(\varepsilon) \approx \rho_{5f}(\varepsilon) = 2 \sum_h \sum_{m_h} |c_{5f m_h}^h|^2 \delta(\varepsilon - \varepsilon_h), \quad (11)$$

which includes the electron spin degeneracy. This PDOS is plotted in Fig. 3 (red curve). Since the DOS $\rho(\varepsilon) = 2 \sum_h \delta(\varepsilon - \varepsilon_h)$, we may relate the DOS and PDOS as

$$\rho_{5f}(\varepsilon_h) \approx \rho(\varepsilon_h) \sum_{m_h} |c_{5f m_h}^h|^2 = 7\rho(\varepsilon_h) \langle |c_{5f}^h|^2 \rangle \quad (12)$$

in the assumption of slowly varying expansion coefficients over energy and the introduction of an average value $\langle |c_{n\ell}^h|^2 \rangle = \sum_m |c_{n\ell m}^h|^2 / (2\ell + 1)$.

With the hole-state expansion (10) and the HFI matrix element (9), the IC rate simplifies to

$$\Gamma_{\text{IC}} = \frac{2\pi}{2I_e + 1} \rho(\varepsilon_{h_r}) \sum_{m_h} |c_{5f m_h}^h|^2 \quad (13)$$

$$\times \sum_{m_d m_e m_g m_s m'_s} |\langle g m_g | \boldsymbol{\mu} | e m_e \rangle \cdot \langle 5f m_d m_s | \mathbf{T} | 5f m_h m'_s \rangle|^2,$$

where the h_r superscript in the expansion coefficients has been dropped.

Since the HFI matrix elements are accumulated near the nucleus and Th electrons in this region ($\alpha Z \approx 0.65$ for $Z = 90$ of Th) are relativistic, we derived the relativistic generalization of the expression (13), where we distinguish between two fine-structure components of the $5f_j$ state, $j = 5/2$ and $j = 7/2$, as

$$\Gamma_{\text{IC}} = \frac{2\pi\rho(\varepsilon_{h_r})}{3(2I_e + 1)} |\langle g | \boldsymbol{\mu} | e \rangle|^2 \times \sum_{j_d j_h} |\langle 5f_{j_d} | \mathbf{T} | 5f_{j_h} \rangle|^2 \langle |c_{5f_{j_h}}|^2 \rangle. \quad (14)$$

Here, the Wigner-Eckart theorem and the averages $\langle |c_{5f_{j_h}}|^2 \rangle \equiv \sum_{m_h} |c_{5f_{j_h} m_h}|^2 / (2j_h + 1)$ have been used to simplify the expression. Since VASP is a non-relativistic code, we relate this average to the non-relativistic expansion coefficient $c_{n\ell m_l}$, c.f. Eq. (10), using the angular momentum algebra

$$\langle |c_{n\ell j}|^2 \rangle = \frac{1}{2j + 1} \sum_{m_l} |c_{n\ell m_l}|^2 \sum_{m_j} |C_{\ell m_l, s m_s}^{j m_j}|^2, \quad (15)$$

where $C_{\ell m_l, s m_s}^{j m_j}$ are the Clebsch-Gordan coefficients with $s = 1/2$ and $\ell = 3$. For an isotropic environment, $|c_{n\ell m_l}|^2 = \langle |c_{n\ell}|^2 \rangle$, so that Eq. (15) simplifies to $\langle |c_{n\ell j}|^2 \rangle = \langle |c_{n\ell}|^2 \rangle / 2$. Thereby, $\langle |c_{5f_{7/2}}|^2 \rangle = \langle |c_{5f_{5/2}}|^2 \rangle = \langle |c_{5f}|^2 \rangle / 2$.

We computed the required hyperfine matrix elements using our *ab initio* relativistic atomic-structure code with random-phase-approximation and Brueckner-orbital many-body contributions [19, 20]. The results are (in atomic units): $\langle 5f_{5/2} | \mathbf{T} | 5f_{5/2} \rangle = 0.29$, $\langle 5f_{7/2} | \mathbf{T} | 5f_{7/2} \rangle = 0.17$, $\langle 5f_{7/2} | \mathbf{T} | 5f_{5/2} \rangle = -0.097$. This implies that with a $\sim 20\%$ accuracy we may retain only the $j_h = j_d = 5/2$ contribution to the rate (14).

Then the IC rate can be expressed in terms of the hyperfine structure constant $A_{5f_{5/2}}$ for the $^{229}\text{Th}^{3+}$ $5f_{5/2}$ ground state with the nucleus in its ground state by employing the relation [18]

$$A_{5f_{5/2}} = \frac{2}{5} \sqrt{\frac{2}{105}} \mu_g \langle 5f_{5/2} | \mathbf{T} | 5f_{5/2} \rangle, \quad (16)$$

leading to an expected IC rate of

$$\Gamma_{\text{IC}} \approx \frac{2\pi}{\hbar} \xi \rho_{5f}(\varepsilon_{h_r}) (A_{5f_{5/2}})^2. \quad (17)$$

Here ξ is the dimensionless geometric factor

$$\xi = \frac{125 \langle |c_{5f_{5/2}}|^2 \rangle |\langle g | \boldsymbol{\mu} | e \rangle|^2}{32 \langle |c_{5f}|^2 \rangle \mu_g^2}, \quad (18)$$

with $\mu_g = 0.360(7)\mu_N$ being the magnetic moment of the ground nuclear state [21] and $\langle g | \boldsymbol{\mu} | e \rangle = 0.84\mu_N$ where μ_N is the nuclear magneton (see SI). As an estimate, in an isotropic environment, $\langle |c_{5f_{5/2}}|^2 \rangle / \langle |c_{5f}|^2 \rangle = 1/2$, resulting in $\xi \approx 11$.

Using the measured value [22] of the $5f_{5/2}$ hyperfine constant is $A_{5f_{5/2}} = 82.2(6)$ MHz, the IC decay rate in practical units is:

$$\Gamma_{\text{IC}} \approx 1.2 \times 10^4 \frac{\rho_{5f}(\varepsilon_{h_r})}{\text{states/eV}} \text{ s}^{-1}, \quad (19)$$

where $\rho_{5f}(\varepsilon_{h_r})$ is the Th impurity f -state PDOS (expressed as the number of states per eV) at the position of the resonant hole $\varepsilon_{h_r} = \varepsilon_d - \omega_{\text{nuc}} - E_R$.

The IC rate (19) depends on the Th impurity f -state PDOS ρ_{5f} . We estimate the PDOS order of magnitude by dividing PDOS integrated over the valence band by a typical few eV width of the valence band (our DFT yields the width of ≈ 3.5 eV for LiSrAlF_6 and ≈ 3 eV for CaF_2 , see Figs. 3 and S2). The integrated PDOS has a meaning of the effective number of Th f -electrons contributing to the valence band. Qualitatively, in ionic hosts, the valence band electrons scatter off of Th^{4+} core, so the integrated PDOS ~ 1 and we expect $\rho_{5f} \sim 0.1$ state/eV in agreement with our DFT calculations for both $^{229}\text{Th}:\text{LiSrAlF}_6$ and $^{229}\text{Th}:\text{CaF}_2$. This estimate leads to $\Gamma_{\text{IC}} \sim 10^3 \text{ s}^{-1}$. Thereby, if the IC process is energetically allowed in solid-state hosts, it quenches the ^{229}Th isomer on a millisecond timescale, much faster than the isomer's measured [2, 3] $\sim 10^3$ s radiative lifetime in solid-state hosts.

While we used the DFT calculations as an important qualitative guide in our derivation of the IC rate, predicting if the IC channel is open critically depends on the reliability of computing the defect state energies ε_d . This may require going beyond DFT methods that typically underestimate excited state energies. A recent CASPT2 study of $\text{Th}:\text{CaF}_2$, using a cluster model with point charge and *ab initio* model potential embedding, found defect state energies of ~ 11 eV, i.e. above ω_{nuc} , for relevant thorium environments [23].

To summarize, if the IC process is energetically allowed, it rapidly quenches the excited nucleus. The recent experiments [2, 3, 5] relied on observing a nuclear decay on a much longer time-scale. We conclude, that in these experiments, the IC was avoided and the doping sites contributing to the observed fluorescence had either

- (i) a sufficiently *high* energy of the defect state, $\varepsilon_d > \omega_{\text{nuc}}$, or
- (ii) a sufficiently *low* energy of the defect state, so that the resonant hole energy lies in the bandgap between valence bands (e.g., below the valence band minimum, $\varepsilon_d - \varepsilon_{\text{min}} > \omega_{\text{nuc}}$.)

The condition (i) has been discussed in the literature, see e.g., Ref. [11] where it is referred to as the ‘‘preserving the band gap’’. The condition (ii) is new - for example, it would have been satisfied if the resonant hole energy ended up in the -3.6 eV -4 eV gap or below -4.5 eV on the Th PDOS plot, Fig. 3.

ACKNOWLEDGEMENTS

This work was supported by NSF awards PHYS-2013011 and PHY-2207546, and ARO award W911NF-11-1-0369. This work used Bridges-2 at Pittsburgh Supercomputing Center through allocation PHY230110 from the ACCESS program, which is supported by NSF grants #2138259, #2138286, #2138307, #2137603, and #2138296.

Supplementary information

Density functional theory methods

DFT calculations were performed with VASP [24], version 6.3, using the PAW [25] method with a plane-wave cutoff of 500 eV and a spin-restricted formalism. The lowest-energy geometry for a Th atom in a supercell of LiSrAlF_6 was determined by screening structures from a previous study of thorium-doped LiCaAlF_6 [26]. 1625 structures of Th:LiCaAlF_6 , in $2 \times 2 \times 1$ supercells of the host material, were converted to Th:LiSrAlF_6 , using optimized lattice parameters for pure LiSrAlF_6 , and reoptimized. Energy corrections to account for differences in stoichiometry were computed using optimized structure energies of binary and ternary fluorides of Li, Sr, and Al. The lowest energy defect geometry was found to be Th replacing Sr with two interstitial F atoms for charge balancing. This structure was expanded to a $3 \times 3 \times 2$ supercell of LiSrAlF_6 and reoptimized. All electronic structure properties were computed for this $3 \times 3 \times 2$ supercell. The PBE [27] functional was used for all structural optimizations, and the modified Becke-Johnson (MBJ) [28, 29] functional was used for electronic properties. Optimizations of $2 \times 2 \times 1$ supercells were done with a 4-4-4 k -point grid, and electronic structure calculations on the $3 \times 3 \times 2$ supercell used a 4-4-2 k -point grid unless otherwise specified. This large grid was previously determined to be necessary for accurate density of states computations [3]. Integration of the PDOS was done with the trapezium integration function in numpy.

Calculations on Th:CaF_2 were done using a $3 \times 3 \times 3$ supercell of the conventional unit cell of CaF_2 . The thorium atom was put on a Ca site and two fluorine atoms were added to compensate the charge in the 90° configuration. This has been found to be the lowest energy geometry in previous investigations and our own calculations.[17]

The phonon analysis required optimization of an excited electronic state of Th:LiSrAlF_6 . To emphasize the local nature of the non-periodic Th defect environment, excited state optimizations were done with only the thorium atom and either 9 or 12 fluorine atoms free to move. The excited state optimizations were done in a $2 \times 2 \times 1$ supercell of Th:LiSrAlF_6 with the same local Th environment as in the larger supercells used in this study, using the Γ point only. The first electronic excited state was reached by fixing the occupancies of the Kohn-Sham orbitals such that an electron was promoted from the highest occupied orbital of the ground electronic state to the lowest unoccupied orbital of the ground state. The first excited state, rather than an excited state on resonance with the nuclear transition, was used to ease excited state SCF convergence. Both excited states involve F-Th electron transfer so they can be expected to have similar lattice relaxation parameters. These calculations used

an unrestricted Kohn-Sham wavefunction ansatz. This is in the spirit of Δ -SCF and was done in VASP using the ISMEAR settings. Relaxation energies for Huang-Rhys theory analysis were computed by recalculating the ground electronic state at the optimized geometry of the excited state, and then taking the energy difference between that and the equilibrium geometry for the ground electronic state.

Additional computational figures

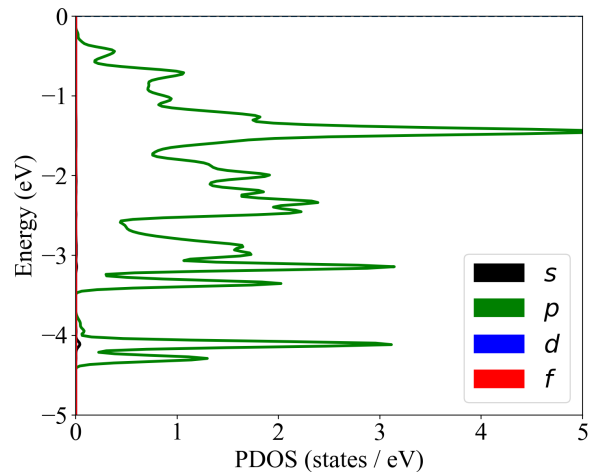


FIG. 4. Fluorine projected density of states in the valence band for a F atom in Th:LiSrAlF_6 .

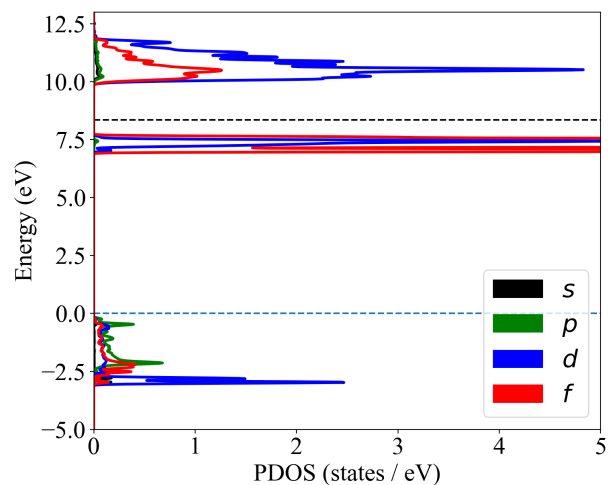


FIG. 5. Thorium projected density of states in the for Th:CaF_2 . The black dashed line marks the nuclear transition energy relative to the top of the valence band.

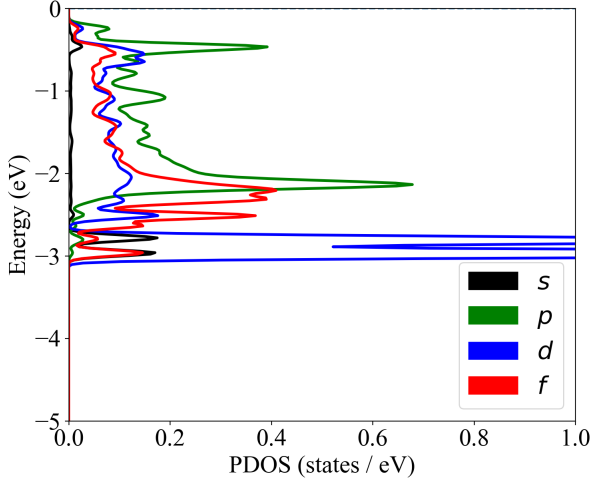


FIG. 6. Thorium projected density of states in the valence band for Th:CaF₂.

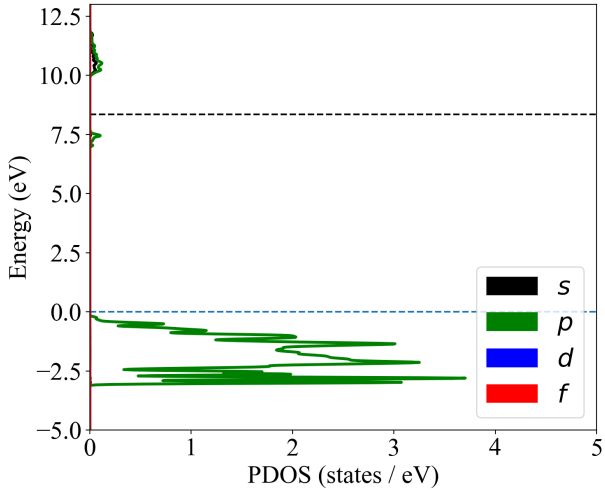


FIG. 7. Fluorine projected density of states for a F atom in Th:CaF₂. The black dashed line marks the nuclear transition energy relative to the top of the valence band.

Combining measurements of lifetime

The new measurements [2, 3] of the energy and radiative lifetime of the 229-Th isomeric state imply an estimate for the M1 matrix element for 229-Th somewhat different from its current value of $\langle g||\mu||e \rangle = 1.2\mu_N$ [30, 31]. While there is very good agreement between Refs. [2] and [3] on the isomeric state energy of $\omega \approx 8.355$ eV, their values for the isomeric lifetime, $\tau = 2510 \pm 72$ s and $\tau = 1860 \pm 79$ s differ significantly. To get an estimate for $\langle g||\mu||e \rangle$, we seek to combine these two values for τ .

One may adopt a simple approach for a weighted av-

erage and chi-squared-rescaled uncertainty where

$$\tau = \frac{w_1\tau_1 + w_2\tau_2}{w_1 + w_2}, \quad (20a)$$

$$\chi^2 = w_1(\tau_1 - \tau)^2 + w_2(\tau_2 - \tau)^2, \quad (20b)$$

$$\sigma^2 = \frac{\chi^2}{w_1 + w_2}, \quad (20c)$$

with $\tau_1 = 2510$ s, $\tau_2 = 1860$ s, $w_1 = 1/\sigma_1^2 = 1/72$ s⁻², and $w_2 = 1/\sigma_2^2 = 1/79$ s⁻². This however, assumes similar confidence in the measurements.

Since the measurement of τ depends on knowledge of the crystal index of refraction, which is much better characterized for CaF₂ [2] than for LiSrAlF₆ [3], we rescale the weight w_1 by a factor $k > 1$. Here, we pick $k = 2$, thus obtaining

$$\tau = 2319 \pm 296 \text{ s}. \quad (21)$$

Using $\tau = 3/(\omega^3 \langle g||\mu||e \rangle^2)$, one thus finds

$$\langle g||\mu||e \rangle = (0.84 \pm 0.11)\mu_N. \quad (22)$$

* andrei@unr.edu

- [1] W. G. Rellergert, D. DeMille, R. R. Greco, M. P. Hehlen, J. R. Torgerson, and E. R. Hudson, *Phys. Rev. Lett.* **104**, 200802 (2010).
- [2] J. Tiedau, M. V. Okhapkin, K. Zhang, J. Thielking, G. Zitzer, E. Peik, F. Schaden, T. Pronebner, I. Morawetz, L. Toscani De Col, *et al.*, *Phys. Rev. Lett.* **132**, 182501 (2024).
- [3] R. Elwell, C. Schneider, J. Jeet, J. E. S. Terhune, H. W. T. Morgan, A. N. Alexandrova, H. B. Tran Tan, A. Derevianko, and E. R. Hudson, *Phys. Rev. Lett.* **133**, 013201 (2024).
- [4] C. Zhang, L. von der Wense, J. F. Doyle, J. S. Higgins, T. Ooi, H. U. Friebel, J. Ye, R. Elwell, J. E. S. Terhune, H. W. T. Morgan, A. N. Alexandrova, H. B. T. Tan, A. Derevianko, and E. R. Hudson, (2024), arXiv:2410.01753.
- [5] C. Zhang, T. Ooi, J. S. Higgins, J. F. Doyle, L. von der Wense, K. Beeks, A. Leitner, G. A. Kazakov, P. Li, P. G. Thirolf, T. Schumm, and J. Ye, *Nature* **633**, 63 (2024).
- [6] F. F. Karpeshin and M. B. Trzhaskovskaya, *Phys. Rev. C* **76**, 1 (2007).
- [7] E. V. Tkalya, C. Schneider, J. Jeet, and E. R. Hudson, *Phys. Rev. C* **92**, 054324 (2015).
- [8] P. V. Bilous, G. A. Kazakov, I. D. Moore, T. Schumm, and A. Pálffy, *Physical Review A* **95**, 1 (2017).
- [9] P. V. Bilous, N. Minkov, and A. Pálffy, *Phys. Rev. C* **97**, 2 (2018).
- [10] E. V. Tkalya, C. Schneider, J. Jeet, and E. R. Hudson, *Phys. Rev. C* **92**, 054324 (2015), arXiv:1509.09101.
- [11] S. V. Pineda, P. Chhetri, S. Bara, Y. Elskens, S. Casci, A. N. Alexandrova, M. Au, M. Athanasakis-Kaklamanakis, M. Bartokos, K. Beeks, C. Bernerd,

- A. Claessens, K. Chrysalidis, T. E. Cocolios, J. G. Correia, H. De Witte, R. Elwell, R. Ferrer, R. Heinke, E. R. Hudson, F. Ivandikov, Y. Kudryavtsev, U. Köster, S. Kraemer, M. Laatiaoui, R. Lica, C. Merckling, I. Morawetz, H. W. T. Morgan, D. Moritz, L. M. C. Pereira, S. Raeder, S. Rothe, F. Schaden, K. Scharl, T. Schumm, S. Stegemann, J. Terhune, P. G. Thirolf, S. M. Tunhuma, P. V. D. Bergh, P. Van Duppen, A. Vantomme, U. Wahl, and Z. Yue, , 1 (2024), arXiv:2408.12309.
- [12] A. L. Fetter and J. D. Walecka, *Quantum Theory of Many-particle Systems* (McGraw-Hill, New York, 1971).
- [13] C. Cohen-Tannoudji, B. Diu, F. Laloe, and E. Merzbacher, *Quantum Mechanics*, 3rd ed., Vol. I and II (Wiley, John and Sons, 1998).
- [14] C. Cohen-Tannoudji, J. Dupont-Roc, and G. Grynberg, *Atom-photon interactions: basic processes and applications* (John Wiley & Sons, 1998).
- [15] VASP Software GmbH, Vienna Ab initio Simulation Package (VASP) (2023).
- [16] K. Huang and A. Rhys, Proc. R. Soc. Lond. A **204**, 406 (1950).
- [17] P. Dessovic, P. Mohn, R. Jackson, G. Winkler, M. Schreitl, G. Kazakov, and T. Schumm, Journal of Physics - Condensed Matter **26**, 10.1088/0953-8984/26/10/105402 (2014).
- [18] W. R. Johnson, *Atomic Structure Theory: Lectures on Atomic Physics* (Springer, New York, NY, 2007).
- [19] H. B. Tran Tan and A. Derevianko, Phys. Rev. A **107**, 042809 (2023).
- [20] C. J. Campbell, A. G. Radnaev, A. Kuzmich, V. A. Dzuba, V. V. Flambaum, and A. Derevianko, Phys. Rev. Lett. **108**, 120802 (2012).
- [21] M. S. Safronova, U. I. Safronova, A. G. Radnaev, C. J. Campbell, and A. Kuzmich, Physical Review A **88**, 6 (2013).
- [22] C. Campbell, A. Radnaev, and A. Kuzmich, Phys. Rev. Lett. **106**, 223001 (2011).
- [23] K. Nalikowski, V. Veryazov, K. Beeks, T. Schumm, and M. Krosnicki, An embedding cluster approach for accurate electronic structure calculations of (229)th:caf2 (2024).
- [24] G. Kresse and J. Furthmuller, Physical Review B **54**, 11169 (1996).
- [25] P. E. Blochl, Physical Review B **50**, 17953 (1994).
- [26] M. Pimon, P. Mohn, and T. Schumm, Advanced Theory and Simulations **5**, 10.1002/adts.202200185 (2022).
- [27] J. P. Perdew, K. Burke, and M. Ernzerhof, Physical Review Letters **77**, 3865 (1996).
- [28] F. Tran and P. Blaha, Physical Review Letters **102**, 10.1103/PhysRevLett.102.226401 (2009).
- [29] A. D. Becke and E. R. Johnson, Journal of Chemical Physics **124**, 10.1063/1.2213970 (2006).
- [30] A. M. Dykhne and E. V. Tkalya, JETP Lett. **67**, 251 (1998), [Pis'ma Zh. Éksp. Teor. Fiz. 67, 233–238 (1998)].
- [31] S. G. Porsev and V. V. Flambaum, Phys. Rev. A **81**, 032504 (2010).